Proceedings of the ASME/JSME 2011 8th Thermal Engineering Joint Conference
AJTEC2011
March 13-17, 2011, Honolulu, Hawaii, USA

AJTEC2011-44064

EXPERIMENTAL INVESTIGATION OF A SCALED-UP PASSIVE INTERDIGITAL MICROMIXER WITH CIRCULAR-SECTOR MIXING ELEMENTS

Kristina Cook
Department of Mechanical and Industrial Engineering,
Concordia University,
Montreal, Quebec, Canada

YanFeng Fan
Department of Mechanical and Industrial Engineering,
Concordia University,
Montreal, Quebec, Canada

Ibrahim Hassan
Department of Mechanical and Industrial Engineering,
Concordia University,
Montreal, Quebec, Canada

ABSTRACT

Flow patterns and mixing phenomena are investigated qualitatively in a planar passive scaled-up micromixer using flow visualization over $5 \leq Re \leq 200$. To promote molecular diffusion, the test section utilizes an uneven interdigital inlet which reduces the diffusion path and enhances mixing at the side walls. Five circular sector obstructions located along the channel length serve to divide and recombine the flow, as well as induce Dean vortex formation at high Reynolds numbers. Induced fluorescence is used to provide a quantitative estimate of mixing efficiency at certain Reynolds numbers. A decreasing-increasing trend in mixing efficiency is observed with increasing Reynolds numbers, marking the transition from mass diffusion dominance to mass advection dominance. The design operates well at higher Reynolds numbers, where the dominant mixing mechanism is mass advection.

NOMENCLATURE

C	Concentration [$\mu g \cdot L^{-1}$]
D_{Hcurve}	Hydraulic diameter in the curve [mm]
D_H	Hydraulic diameter [m]
H	Height [mm]
I	Intensity [a.u.]
L	Length [mm]
M	Mixing efficiency
N	Total number of samples
R_{curve}	Centerline radius of curvature [mm]
U	Mean velocity [$m \cdot s^{-1}$]
W	Width [mm]
Greek	
μ	Dynamic viscosity [$kg \cdot m^{-1} \cdot s^{-1}$]
ρ	Density [$kg \cdot m^{-3}$]
Subscripts	
i	Sample *i*
m	Mean
mo	Model
max	Maximum
min	Minimum
p	Prototype

INTRODUCTION

Micromixers are an integral part of micro-lab-on-a-chip and micro-total-analysis systems (μ-TAS), which have applications in the fields of drug delivery, DNA synthesis, and biological and chemical analyses, amongst others. To ensure the amelioration and further development of microsystems, it is essential to develop low cost, easy-implementation micromixers with high mixing efficiency, low pressure drops, and short mixing lengths.

Several reviews of micromixer classifications, mixing mechanisms and applications have been presented in the literature [1-3]. Micromixers are broadly categorized as either passive or active; the later utilize external forces, such as electromagnetic fields [4] and thermal gradients [5] to induce mixing. Active micromixers generally have higher mixing efficiency than passive micromixers; however, they are costly, difficult to implement, and may damage sensitive biological matter. It is worth noting, however, that micromixers operating under high shear may also damage biological samples [6].

Passive micromixers, on the other hand, make use of channel geometry to promote mixing between species, and may be further classified based on one of two main passive mixing principles: molecular diffusion and chaotic advection [7]. To reduce the diffusion path and increase interfacial contact area, several researchers have implemented multi-lamination techniques at the inlet [8-11]. Due to the dependence on diffusion-dominant mixing, parallel lamination mixers work well at low Re. At higher Re, however, chaotic advection dominates. Chaotic advection, characterized by the folding, stretching and breaking up of fluid due to transverse flow, is a widely applied mixing mechanism. In passive micromixers, the implementation of flow separating structures has been used to improve mixing efficiency by inducing vortex formation [12], causing chaotic advection to be the dominant mixing mechanism [13, 14]. Split and recombine techniques were also applied [15] to improve mixing efficiency, whereby each mixing element increased the number of striations exponentially. Ansari et al. [16] designed a micromixer with uneven curved substreams, while Chung and Shih [17] designed a three-rhombus flow dividing micromixer with two constriction elements. Increased inertial and centrifugal forces in the substreams led to improved mixing at higher Reynolds numbers. At low Re, mixing was found to be diffusion dominant, while at higher Re, advection was the primary mixing mechanism.

The present scaled up micromixer, or mini-mixer, is based on the principles of multi-lamination and flow separation techniques, and therefore takes advantage of both molecular diffusion and chaotic advection mechanisms. An interdigital inlet is applied which divides 2 individually supplied species into 3 and 4 substreams, respectively. Five circular sector mixing elements divide and recombine the flow. This allows fluid stream collisions, and promotes Dean vortex generation at high Reynolds numbers. Flow visualization is used to provide insight into the phenomena occurring as species interact at Reynolds numbers ranging from $5 \leq \mathrm{Re} \leq 200$.

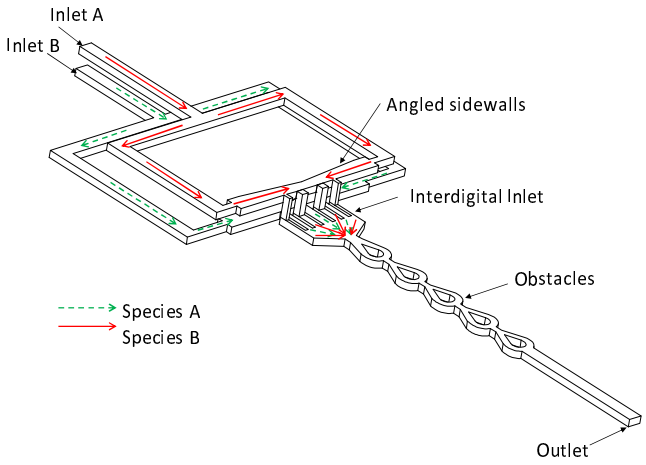

FIGURE 1. TEST SECTION WITH INTERDIGITAL INLET AND CIRCULAR SECTOR ELEMENTS

EXPERIMENT

Test Section

Figure 1 shows the scaled test section used in the present experiment, which consists of three fused cast acrylic layers, in which all channels are machined to a depth of 2 mm using CNC machining. To enhance mixing efficiency by increasing interfacial contact area and decreasing diffusion path, an interdigital inlet is applied. As shown in the fig. 1, species A enters via the upper inlet where it is divided into 4 uneven lamellae and directed towards the bottom layer via 4 through holes. Species B enters via the lower inlet, where it is divided into 3 uneven lamellae. The channel side walls are angled to ensure fluid flows though each substream. The species streams are rapidly converged upon entering the mixing region; this forces the fluid flow in a direction parallel to the diffusion path, which serves to increase the effects of Taylor dispersion. The 7 lamellae are then directed toward the first of 5 circular sector mixing elements. These elements serve to split and recombine the fluid. Before approaching each mixing element, the fluids collide, are converged, diverged and split by the next element. The curved portion around the circular element induces mixing by taking advantage of the centrifugal forces of the fluid, thereby promoting the generation of Dean vortices. Figure 2 shows important test section dimensions.

Dimensional Similarity

To maintain dynamic similarity between the model, *mo*, and prototype, *p*, the Reynolds number,

$$Re = \frac{\rho U D_H}{\mu} \tag{1}$$

is kept constant. Given the same fluid under the same operating conditions, the above equation reduces to

$$UD_H\Big|_{mo} = UD_H\Big|_{p} \tag{2}$$

where ρ, D_H, U and μ represent the density, hydraulic diameter, average velocity and viscosity, respectively. To preserve geometric similarity, equations (3-5) must be respected.

$$\frac{D_H}{L}\Big|_{mo} = \frac{D_H}{L}\Big|_{p} \tag{3}$$

$$\frac{H}{L}\Big|_{mo} = \frac{H}{L}\Big|_{p} \tag{4}$$

$$\frac{W}{L}\Big|_{mo} = \frac{W}{L}\Big|_{p} \tag{5}$$

where L is the channel length, and H and W represent the channel height and width at a given location.

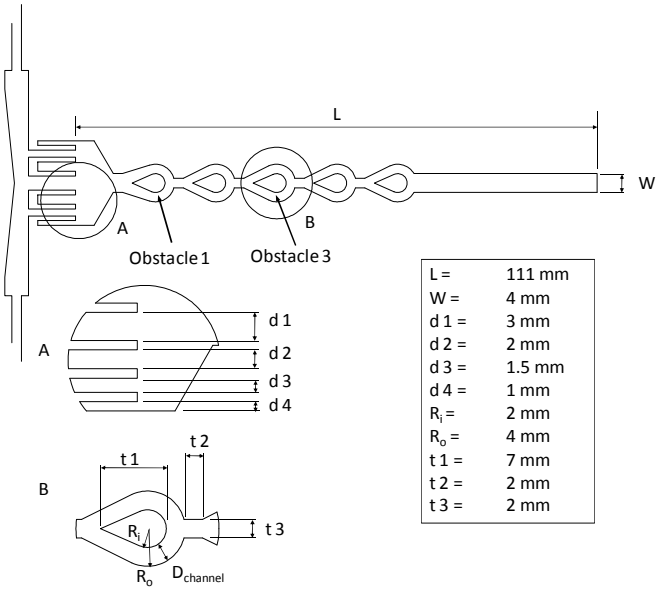

FIGURE 2. DETAILS AND DIMENSIONS OF TEST SECTION

Experimental Facilities

The experimental facility is shown in fig. 3. For flow visualization measurements, a 3CCD (Sony CDX-9000) camera, along with appropriate lighting, is located above the test section. Two syringe pumps (New Era Pump Systems Inc., model NE-1010), which are digitally set to the required flow rate, individually supply two species to the test section. For induced fluorescence measurements, the test section is positioned on a microscope stage (Nikon Eclipse TE2000-S). A mercury lamp (Chiu Technical Corporation, Mercury 100 W) supplies continuous light with a peak of approximately 532 nm through a 2 × objective lens to the test section. Emission light from the test section is directed through an Epi-fluorescence filter, where light with a peak wavelength of approximately 610 nm is captured by a CCD camera (Dantec Dynamics - HiSense MkII).

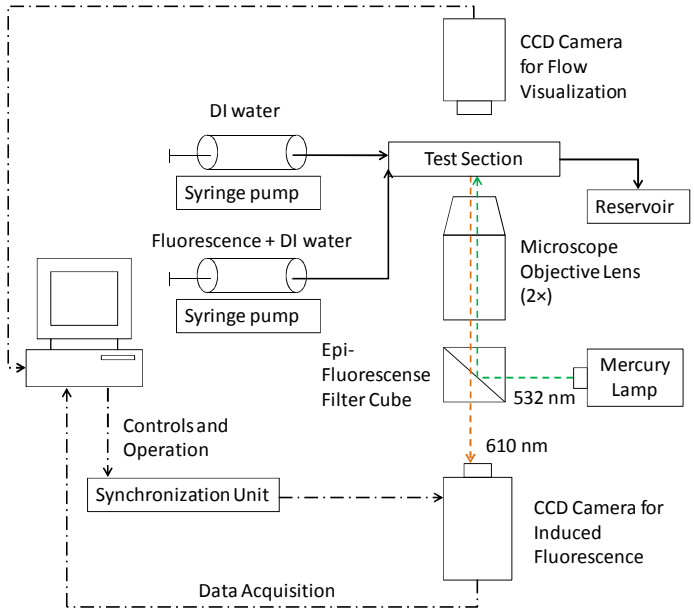

FIGURE 3. EXPERIMENTAL FACILITY

Experimental Methodology

For flow visualization experiments, solutions of water with red and green food colours are supplied separately and simultaneously to the test section via two syringe pumps. Images are captured at flow rates ranging from $5 \leq Re \leq 200$, where the Reynolds number is calculated based on the hydraulic diameter of the mixing entrance region. The corresponding Dean number, Dn, calculated in the vicinity of the curved obstacles and based on the curved channel Reynolds number, Re_{curve}, is defined as [18]:

$$Dn = Re_{curve}\sqrt{\frac{D_{H\,curve}}{R_{curve}}} \tag{6}$$

and varies from $4.08 \leq Dn \leq 122.5$. In the above equation, D_{Hcurve} is the hydraulic diameter of the curved channel and R_{curve} is the centerline radius of curvature.

Induced fluorescence is performed to obtain quantitative mixing efficiency results. Distilled water is combined with Rhodamine 6G to create solutions with concentrations ranging from 0 to 1400 µg/L. Prior to experimentation, calibration is performed to ensure that the concentrations of species used in the experiments are located in the linear range of the concentration-intensity curve. Based on the calibration curve, a given light intensity is associated with a given concentration according to

$$I_i = \frac{I_{\max} - I_{\min}}{C_{\max} - C_{\min}} \tag{7}$$

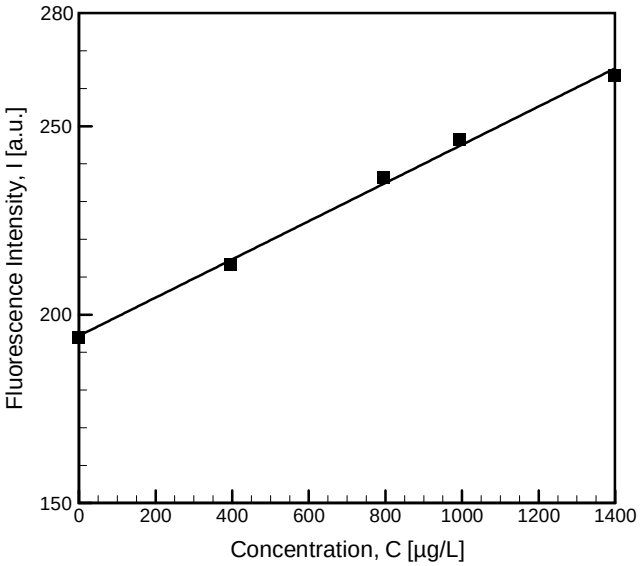

FIGURE 4. SAMPLE CALIBRATION CURVE

In the above equation, I represents the intensity and C represents the concentration. Subscripts i, max and min represent sample i, maximum and minimum, respectively. A sample calibration curve depicting the relationship between fluorescence intensity and concentration is shown in figure 4. To reduce errors, operating parameters, namely measurement plane and light intensity, are kept constant throughout the calibration and experimentation process. While focusing on the center plane using the Bino mode, 50 images of 1344 × 1024 pixels are captured at intervals of 0.05s and processed and averaged using Flow Manager Software. Greyscale images are converted to concentration values based on the concentration-intensity curve determined in the calibration process.

RESULTS AND DISCUSSION

Flow Visualization

Figure 5 shows flow visualization results at Re = 5, 25, 100 and 200 for obstacles 1, 3 and the outlet. As the present test section is scaled up, conventional CNC methods were used in fabrication and bonding. Bonding difficulties led to shadows present at certain positions along the test section, as may be seen in fig. 5.

For all Reynolds numbers tested, 7 lamellae are visible at the entrance to the first obstacle. At Re= 5, the lamellae remain undistorted along the obstacle length. At increased Reynolds numbers, however, a mixed region is visible behind the obstacle, as shown in fig. 5 A, C and E. This apparent mixed region is likely due to the development of Dean vortices, which occur as fluid moves around the curved portion of the obstacles. The fluid in the center of the channels has higher velocity and centrifugal force than does the fluid closer to the walls. For this reason, fluid at the center is forced outward as is flows around a curved surface. As shown in fig. 5, the magnitude of the mixed region increases with increasing Reynolds number, as expected. The formation of Dean vortices is credited with the superior mixing performance at high Reynolds numbers. At main channel Re = 200, the corresponding Dean number is 86.6. It should be noted that the Dean number is based on the Reynolds number in the curved channel. Several authors have reported the formation of Dean vortices in curved channels [18, 19]. As a basis for comparison, weak helical motion was observed by Jiang et al. (2004) at Dn = 10; the helical flow increased with increasing Dn, such that two counter-rotating vortices were observed. Howell et al. (2004) also reported the presence of counter-rotating vortices at Re = 16-30. The commonly reported critical Dean number of Dn ≈ 140, where four counter rotating vortices appear [references, 18], was not tested. As flow visualization is an optical technique, it is important to note that as a fluid interface tilts, mixing may appear more thorough that it actually is. Figure 5 E depicts an interesting phenomenon: stagnant red species is seen directly behind the obstacle, as opposed to the green species seen at lower Re. This may be due to species interface oscillations, as well as the formation of an apparent stagnant zone behind the obstacle. The frequency and amplitude of the oscillations increases with increasing Reynolds number. Comparison with previous work (T-inlet) [20] shows that the use of the interdigital inlet

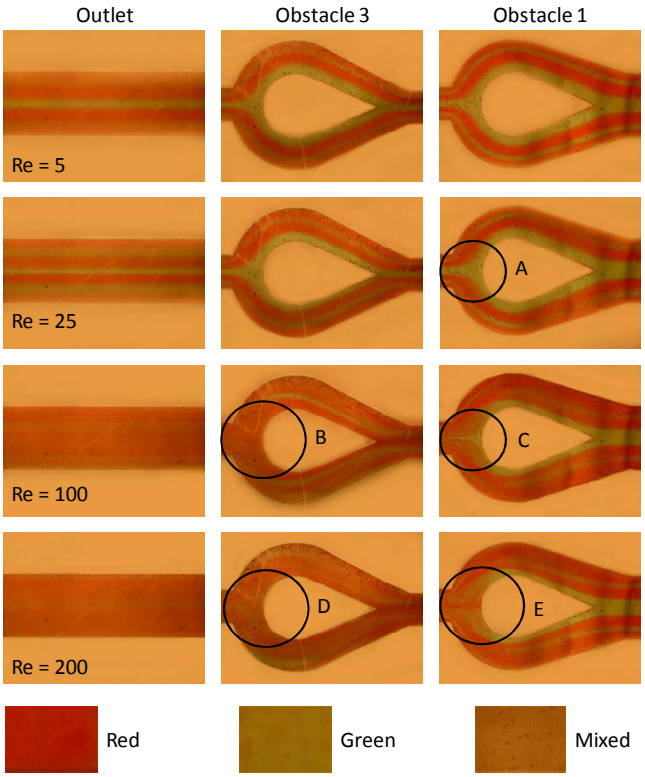

FIGURE 5. FLOW VISUALIZATION RESULTS AT THREE POSITIONS AT RE = 5, 25, 100 AND 200

considerably reduces the appearance of oscillations. A comparison of locations B – C and D – E demonstrates a substantial increase in mixing efficiency with increasing obstacle number. As seen from the images at the outlet, superior mixing is achieved at high Re (Re = 100 and 200). At Re = 25, 7 lamellae remain clearly visible, whereas at Re = 5, the lamellae at the side wall are not clearly distinguished. Side wall mixing is enhanced due to the uneven interdigital inlet, where the diffusion path is reduced. Reduction in diffusion path is particularly beneficial at low Re, where mixing is diffusion dominant. These results indicate a decreasing-increasing trend in mixing efficiency with increasing Reynolds number. The dominant mixing mechanism, therefore, changes from diffusion to advection, with a critical point (among tested values) at Re = 25.

Induced Fluorescence

Figure 6 presents induced fluorescence images at the outlet at Re = 25 and Re = 50. As shown in the figure, mixing is enhanced at Re = 50, as compared to Re = 25. As shown in the flow visualization results, all 7 lamella are visible at Re = 25. When advection becomes dominant, mixing is enhanced, as evidenced by the comparatively higher concentration at the side walls, and lower concentration in the center region.

The mixing efficiency, M, is defined by

$$M = 1 - \sqrt{\frac{1}{N}\sum_{i=1}^{N}\left(\frac{C_i - C_m}{C_m}\right)^2} \quad (8)$$

where

$$C_m = \frac{\sum_{i=1}^{N} C_i}{N} \quad (9)$$

In the above equations, N is the total number of samples, i is the sample number, C_i is the concentration at sample i, and C_m is the mean concentration. Based on the above definitions, M = 0.538 at Re = 25, and M = 0.643 at Re = 50. At high Re, symmetric oscillations of the species interface were apparent along the center of the channel. As such, averaging IF measurements at high Re would over predict mixing efficiency. It should be noted that manufacturing defects, such as surface scratches and shadows caused by the bonding agent may cause errors related to light reflection.

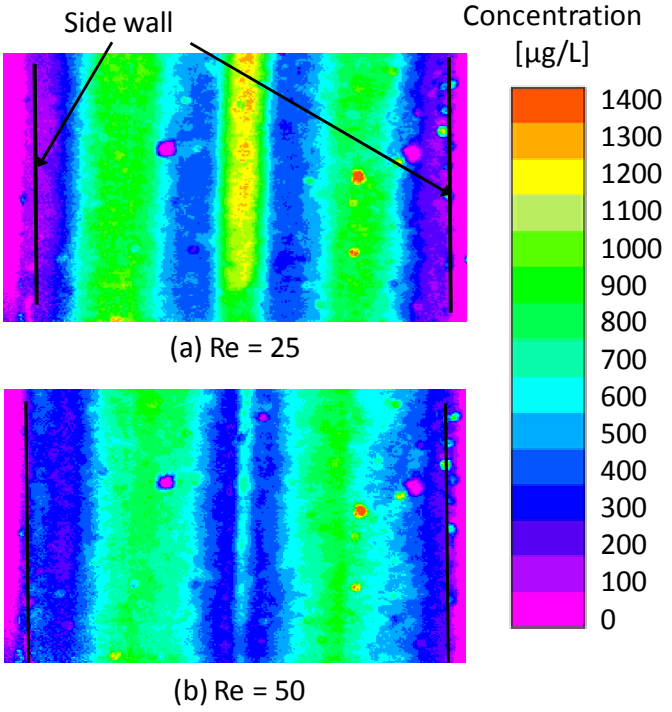

FIGURE 6. IF RESULTS AT THE OUTLET AT RE = 25 AND RE = 50

CONCLUSIONS

Based on flow visualization results, the present scaled micromixer exhibits superior mixing at high Reynolds numbers. A decreasing-increasing trend in mixing efficiency is observed with increasing Reynolds numbers, which signifies the change in the dominant mixing mechanism. At lower Reynolds numbers, mixing is diffusion dominant, while at higher Reynolds numbers, advection dominates. The current design uses geometry to take advantage of Taylor dispersion at the entrance to the mixing region, as well as Dean vortex generation along the curved surface of the obstacles. The interdigital inlet not only increases mixing performance by reducing the diffusion path, it reduces oscillations caused by the use to two separate pumps by supplying fluids parallel to each other.

Future numerical work would allow for the mixing mechanisms and flow patterns to be analyzed in greater detail.

REFERENCES

[1] Nguyen, N. T, Wu, Z., 2005, "Micromixers- a review", *Journal of Micromechanics and Microengineering*, **15**, R1-R16

[2] Hessel, V., Löwe, H., Schönfeld, F., 2005, "Micromixers- a review on passive and active mixing principles", *Chemical Engineering Science*, **60**, 2479-2501

[3] Aubin, J., Ferrando, M., Jiricny, V., 2010, "Current methods for characterising mixing and flow in microchannels", *Chemical Engineering Science*, **65**, 2065-2093

[4] Lee, S. H., Kang, H. J., Choi, B., 2009, "A study on the novel micromixer with chaotic flows", *Microsyst. Technol*., **15**, 269-277

[5] Tsai. J. H. and Lin, L., 2002, "Active microfluidic mixer and gas bubble filter driven by thermal bubble micropump", *Sensors and Actuators*, **A** (97-98), 665-671

[6] Yang, S. Y., Lin, J. L., Lee, G. B., (2009) "A vortex-type micromixer utilizing pneumatically driven membranes", *J. Micromech. Microeng*., **19,** 9pp

[7] Hardt, S., Schönfeld, F., 2007, *Microfluidic technologies for miniaturized analysis systems*, Springer, Chap. 2

[8] Adeosun, J. T., Lawal, A., 2009, "Numerical and experimental mixing studies in a MEMs-based multilaminated/elongated flow micromixer", *Sensors and Actuators*, **B** (139), 637-647

[9] Löb, P., Drese, K. S., Hessel, V., Hardt, S., Hofmann, C., Löwe, H., Schenk, R., Schönfeld, F., Werner, B., 2004, "Steering of Liquid Mixing Speed in Interdigital Micro Mixers-from Very Fast to Deliberately Slow Mixing", *Chem. Eng. Technol*., **27** (3) 340-345

[10] Wu, Z., Nguyen, N. T., 2005, "Convective-Diffusive transport in parallel lamination micromixers", *Microfluid Nanofluid*, **1**, 208-217

[11] Hessel, V., Löwe, H., Schönfeld, F., 2005, "Micromixers- a review on passive and active mixing principles", *Chemical Engineering Science*, **60**, 2479-2501

[12] Lu, Z., McMahon, J., Mohamed, H., Barnard, D., Shaikh, T. R., Mannella, C. A., Wagenknecht, T., Lu, T. M., 2010, "Passive microfluidic device for submillisecond mixing", *Sensors and Actuators*, **B** (144), 301-309

[13] Chen, L., Wang, G.., Lim, C., Seong, G.. H., Choo, J., Lee, E. K., Kang, S. H.; Song, J. M., 2009, "Evaluation of passive mixing behaviours in pillar obstruction poly(dimethylsiloxane) microfluidic mixer using fluorescence microscopy", *Microfluid Nanofluid*, **7**, 267-273

[14] Nguyen, T. N. T, Kim, M. C., Park, J. S., Lee, N. E., 2008, "An effective passive microfluidic mixer utilizing chaotic advection", *Sensors and Actuators*, **B** (132), 172-181

[15] Li, L., Lee, J., Castro, J. M., Yi, A. Y., 2010, "Improving mixing efficiency of a polymer micromixer by use of a plastic shim divider", *J. Micromechanics and. Microengineering*, **20**, 9pp
[16] Ansari, M. A., Kim, K. Y., Anwar, K., Kim, S. M., 2010, "A novel passive micromixer based on unbalanced splits and collisions of fluid streams", *Journal of Micromechanics and Microengineering*, **20**, 10pp
[17] Chung, C. K., Shih, T. R., 2007, "A rhombic micromixer with asymmetrical flow for enhancing mixing", *Journal of Micromechanics and Microengineering*, **17**, 2495-2504
[18] Jiang, F., Drese, K. S., Hardt, S., Kupper, M., Schönfeld, F., 2004, "Helical Flows and Chaotic Mixing in Curved Micro Channels", *AIChE Journal*, **50** (9), 2297-2305
[18] Howell, P. B. Jr., Mott, D. R., Golden, J. P., Ligler, F. S., 2004, "Design and evaluation of a Dean vortex based micromixer", *Lab Chip*, **4**, 663-669
[19] Fan, Y. F., Hassan, I., 2010, "Experimental and Numerical Investigation of a Scaled-up Passive micromixer using Fluorescence Technique", *Experiments in Fluids*, **49**, 733-747